JOURNAL OF MATERIALS SCIENCE 22 (1987) 4484–4498

Optical and scanning electron microscopic and energy-dispersive X-ray analytical studies on some typical surface structures of flux-grown $DyFeO_3$ crystals

P. N. KOTRU, S. K. KACHROO
Department of Physics, University of Jammu, Jammu 180 001, India
B. M. WANKLYN, B. E. WATTS
Department of Physics, Clarendon Laboratory, Oxford University, Oxford, UK

The results of optical, scanning electron microscope and qualitative analysis studies conducted on surface structures displayed by flux-grown $DyFeO_3$ crystals are reported. The crystals were grown from $PbO–PbF_2–B_2O_3$ flux under various conditions. Magnetoplumbite ($PbO \cdot 6Fe_2O_3$) is the most favoured secondary phase. Crystallization of DyOF and $DyBO_3$ on the $DyFeO_3$ crystal surfaces also takes place, almost at the end of $DyFeO_3$ crystal growth. Macro- and micro-disc patterns on $DyFeO_3$ and a rare observation of an elliptical disc of material containing lead are illustrated. Metallic platinum deposited on flux-grown $DyFeO_3$ is reported when the crystals were finally cooled in contact with the flux. Additional secondary phases (material containing lead, platinum, $PbO \cdot 6Fe_2O_3$, $DyBO_3$) and other imperfections (inclusions, cavities, microcrystals) also occur. The addition of V_2O_5 to the flux leads to incorporation of traces of vanadium in the $DyFeO_3$ crystals and $DyVO_4$ as a secondary phase.

1. Introduction

Growth from the fluxed melt is one of the major techniques for the preparation of crystals which may be useful for technology and scientific study. It yields faceted crystals suitable for micromorphological studies. Assessment of crystals in terms of physical and chemical perfection is important for understanding the materials in terms of their perfection and the causes that generate the imperfections. This finally yields vital clues which can help the elimination of imperfections. Surface structural studies have provided useful information in the case of many crystals [1–13]. The authors have reported the precipitation of secondary phases and the generation of other faults during the flux growth of $ErFeO_3$ and $HoFeO_3$ crystals [14, 15].

In this paper we report the results of a detailed study of some significant surface structures on the faces of flux-grown $DyFeO_3$ crystals using optical and electron microscopy and energy-dispersive analysis of X-rays (EDAX) for element analysis.

2. Experimental details

The results reported were obtained on $DyFeO_3$ crystals grown by the flux method under four different growth conditions, shown in Table I.

Typical features on the crystal surfaces were studied using an optical microscope (Neophot-2, CZ make) and a scanning electron microscope (Cambridge Stereoscan SU-10), and qualitative elemental analysis was done using an energy-dispersive X-ray spectrometer attached to the above scanning electron microscope.

3. Results and discussion

3.1. Results on Batch A

Fig. 1 is a built-up picture showing unusual elevated structures appearing as patterns on the {0 0 1} surface of a $DyFeO_3$ crystal. These structures are found in arrays or at isolated sites (Fig. 2) or crowded together (Fig. 3). In Fig. 3 these elevated structures cluster together to form an elevated region spread over a large area on the crystal surface.

Fig. 4 shows a region of Fig. 2 as seen under the SEM. Part of a large raised plateau found as a result of crowding together of the elevated structures is seen in this micrograph. Fig. 5 is a lone elevated feature as seen under SEM, revealing its structure. It has three almost straight sides (one long and two short sides) and a semicircular (curved) side. All the sides slope and almost invariably they show grains of some material sticking to their sloping sides and their extreme ends. These grains are present irrespective of whether the elevated structure is isolated or many of them are crowded together. Fig. 6 is a scanning electron micrograph where the crowded structures exhibit grains on the sloping sides and their terminal ends. Some such structures, when observed under the SEM adjusted for an oblique view, appear as shown in Fig. 7.

Fig. 8 shows one of the terminal ends of the elevated structures at a higher magnification. The

0022–2461/87 $03.00 + .12

TABLE I Starting compositions and furnace programmes

Batch	Starting composition	Crucible volume (cm^3)	Soak temperature (° C)	Soak time (h)	Rate of cooling	Separation from flux	Notes	Crystal product
A	22.9 g Dy_2O_3, 9.8 g Fe_2O_3, 2.4 g B_2O_3, 45.6 g PbO, 64.8 g PbF_2, 1 g PbO_2	50	1290	16	2 K h^{-1} to 850° C, then 100 K h^{-1} to room temperature	By tapping with a hammer; cleaned in 20% aqueous HNO_3 solution	Eutectic crystallization occurred around crystals in the crucibles	$DyFeO_3$ primary phase, up to 3 mm × 3 mm × 1.5 mm
B	4.1 g Dy_2O_3, 1.8 g Fe_2O_3, 13.2 g PbO, 11.2 g PbF_2, 1.1 g PbO_2 (Dy_2O_3 and Fe_2O_3 in stoichiometric proportions)	20	1260	8	1 K h^{-1} to 945° C	Hot-poured by inverting the crucible; cleaned in 20% aqueous HNO_3 solution	Crystals separated from flux before it solidified; a few drops of flux remained on the crystals, and some flux where they were adjacent to the crucible	Crystals of $DyFeO_3$ about 3 mm × 3 mm × 3 mm; the other major phase is DyOF
C	5.1 g Dy_2O_3, 3.8 g Fe_2O_3, 0.6 g B_2O_3, 10.5 g PbO, 9.6 g PbF_2, 1.2 g PbO_2	20	1260	6	1 K h^{-1} to 840° C	As in Batch B	As above	$DyFeO_3$ primary phase up to 3 mm × 3 mm × 3 mm
D	5.2 g Dy_2O_3, 2.2 g Fe_2O_3, 0.65 g B_2O_3, 1.70 g V_2O_5, 10.5 g PbO, 9.6 g PbF_2, 1.2 g PbO_2	20	1260	6	2 K h^{-1} to 890° C	As in Batch B	As above	$DyFeO_3$ crystals up to 5 mm × 5 mm × 5 mm; the other phase is $DyVO_4$

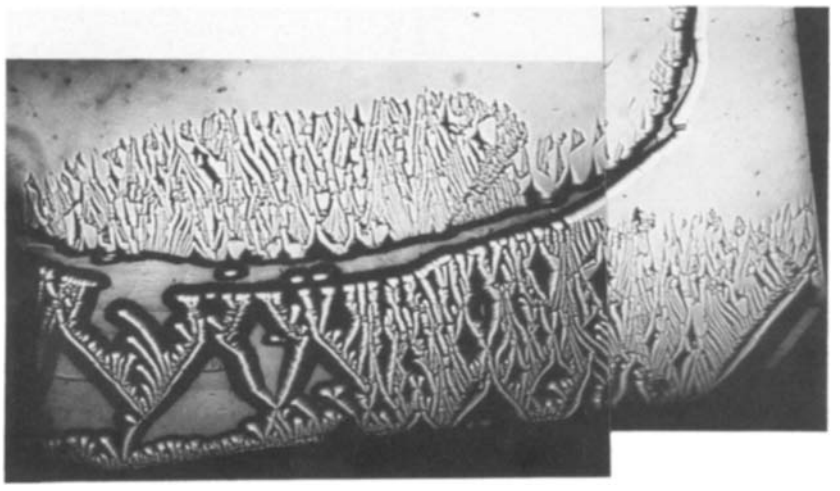

Figure 1 A built-up picture showing elevated structures appearing as imprints on a {0 0 1} surface (× 50).

material sticking to these structures appears in the shape of droplets or small spherical grains. Fig. 9a shows one of many such structures with a white line (A–B–C–D–E) along which an EDAX scan was done. Fig. 9b is the element profile recorded for this feature. The profile reveals the following:

(i) Along AB, both iron and dysprosium are present as on the general plane surface of $DyFeO_3$ (the corresponding peak of iron has not been traced here, for the region AB, to avoid the crowding of peaks).

(ii) Going along BC reveals a region rich in dysprosium and platinum; iron is absent.

(iii) In the region CD there is an absence of platinum but dysprosium is present in varying concentrations.

(iv) The region DE again reveals the presence of platinum and dysprosium in much the same way as along BC.

(v) Although this particular trace shows an absence of lead, this was not so in the case of every such feature. Lead was found present in some cases at the terminals or the sides in combination with platinum and dysprosium.

(vi) It was noted that excepting the region AB, peaks due to iron were absent along the route B–C–D–E.

From the above observations it is inferred that the elevations are rich in dysprosium and contain platinum grains at the tips and on their sides. It is possible that lead precipitates along with dysprosium and platinum. The elevations seem to have formed after the growth of $DyFeO_3$ had ceased and platinum was probably deposited during eutectic crystallization (Batch A being the only batch in which the flux crystallized around the crystals). No evidence was available that these elevations had obstructed or modified the advancing growth fronts of $DyFeO_3$.

The possibility that the above elevated structures might be dysprosium overgrowths is ruled out as it is impossible for dysprosium to be present as a metal in this system, since it is far too reactive. The features could be either DyOF or $DyBO_3$. They disappeared on acid treatment, which excludes the possibility of DyOF. What we, therefore, observe as elevated structures is $DyBO_3$. The precipitation of platinum, which sticks to the sides or at the terminal ends of these elevated structures is a subsequent development and no doubt occurs at eutectic solidification. This is a very interesting finding which has not been reported before.

Fig. 10a shows microcrystals attached as guest crystals on the host surface of growing $DyFeO_3$ (bulk) crystals. As confirmed by EDAX (Fig. 10b), the microcrystals have the same composition as the host crystals and have formed almost at the end of crystal growth when the melt was cooled at about $100\,K\,h^{-1}$ to room temperature. Fig. 11 shows one of the guest microcrystals at a higher magnification, revealing its morphology which is not very different from that of

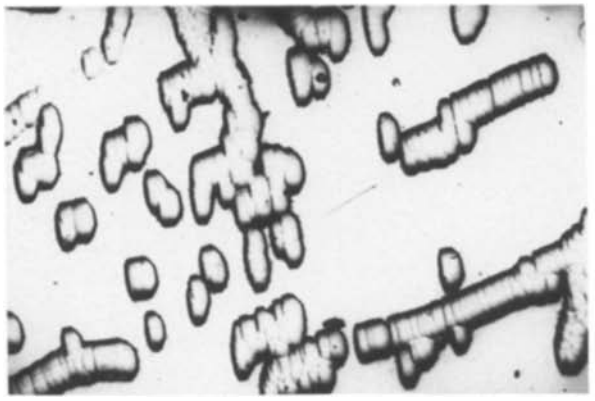

Figure 2 A {0 0 1} surface showing elevated structures at isolated sites and in arrays (× 118).

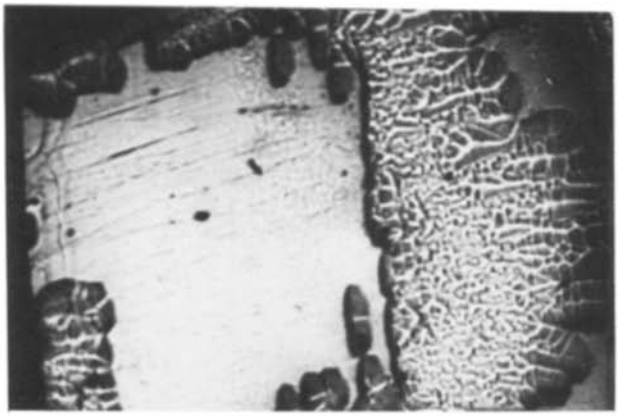

Figure 3 Elevated structures crowded together to form a raised plateau (× 125).

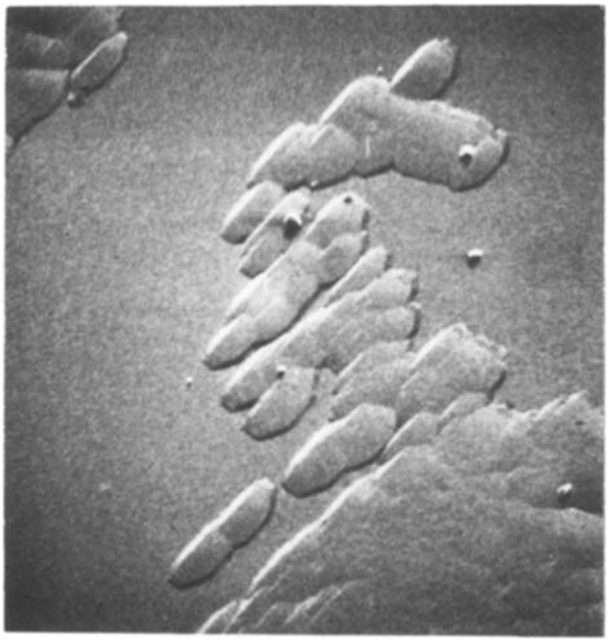

Figure 4 Elevated features of the type shown in Fig. 2 as seen under SEM. Part of a large raised plateau due to crowding of elevated structures is seen (× 89).

the bulk growth. When these are detached from the host surface, they are likely to leave behind depressions and Fig. 12 shows such depressions on the host surface of $DyFeO_3$.

The formation of microcrystals was very often found to be associated with the precipitation of a different phase and Fig. 13a is an electron micrograph showing this material. The precipitate appears as a cluster of small grains. Fig. 13b, the EDAX curve recorded on these grains, reveals the following:

(i) Unlike the general flat surface the grains do not contain peaks due to dysprosium.

(ii) The grains show the presence of lead and iron.

It is inferred that the secondary phase is magnetoplumbite ($PbO \cdot 6Fe_2O_3$), a secondary phase observed with other rare-earth orthoferrites [14, 15].

Figure 5 An electron micrograph showing the finer details of the elevated structure (× 880).

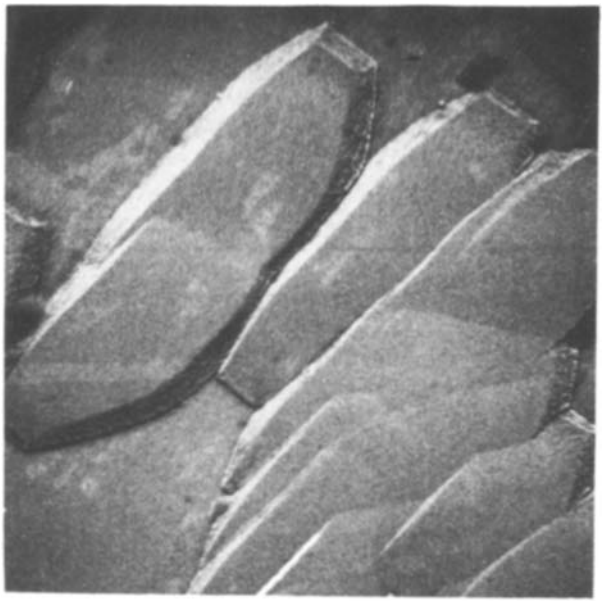

Figure 6 Crowd of elevated structures as seen under the SEM exhibiting grains on their sloping sides and terminal ends (× 450).

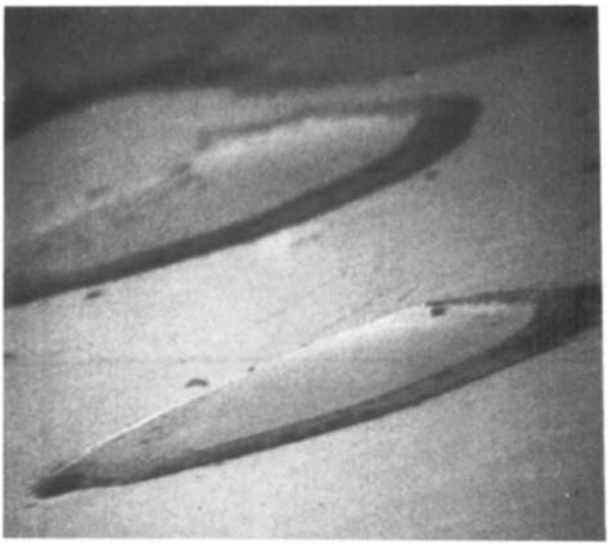

Figure 7 A scanning electron micrograph showing an oblique view of elevated structures (× 910).

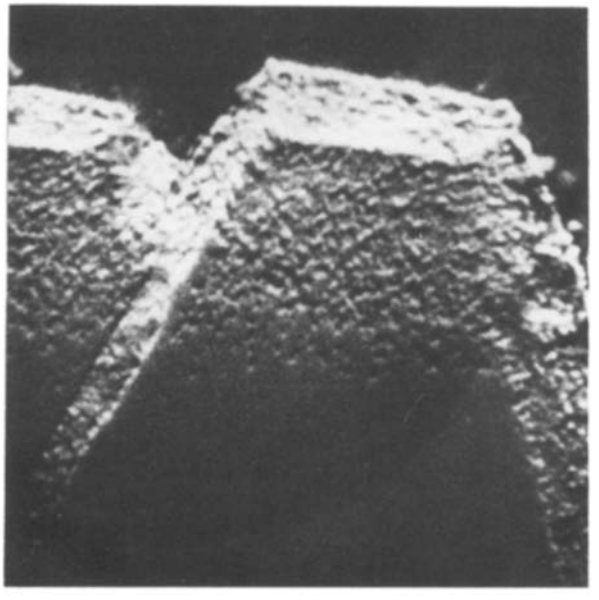

Figure 8 One of the terminal ends of an elevated structure at a higher magnification showing deposition of some material in the shape of droplets or small spherical grains on one of the terminal ends of the elevated structures (× 1820).

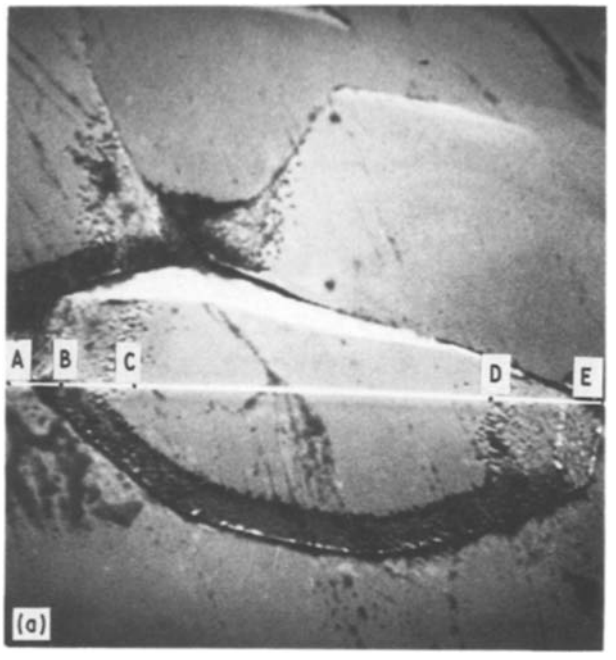

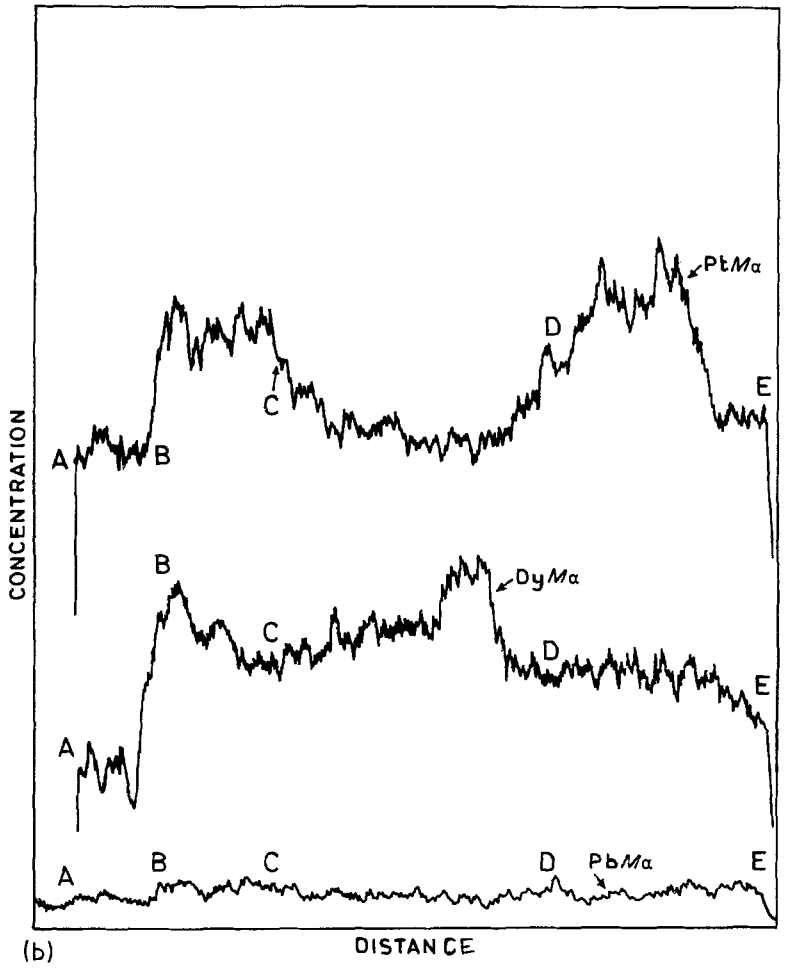

Figure 9 (a) An electron micrograph showing one of the elevated structures along which an elemental profile was recorded. The horizontal white line (A–B–C–D–E) across this figure is the track along which the elemental scan was made (× 735). (b) Element profile traced by EDAX showing detection of Pb$M\alpha$, Dy$M\alpha$ and Pt$M\alpha$ radiation on scanning from left to right along (A–B–C–D–E) of (a). Note the dysprosium- and platinum-rich region along BC, the absence of platinum but presence of dysprosium from C to D, and the platinum- and dysprosium-rich region along DE. (Traces corresponding to Dy$M\alpha$ and Pt$M\alpha$ are separated for convenience.)

The crystals grown in this batch showed some large crystalline inclusions. In Fig. 14, a very large crystalline inclusion, nearly comparable in size with that of the parent $DyFeO_3$ crystal, is shown in a $DyFeO_3$ crystal.

An unusual observation was offered by a $DyFeO_3$ crystal of this batch, recorded in Fig. 15a which shows a typical elliptical microdisc. The white line A–B–C–D across it is the route along which elemental scanning was done. The profile is shown in Fig. 15b. The regions AB and CD, falling outside the disc, are the general surface of $DyFeO_3$ depicting the presence of dysprosium and iron. However, it is clearly indicated in the profile that the region BC (the microdisc) is rich in lead. The microdisc is made of material containing lead, which could be undissolved or incompletely dissolved flux. The possibility of it being made of lead is ruled out as lead dissolves in HNO_3 and has developed after the growth of $DyFeO_3$ had ceased. This is evident from the fact that no growth layers could be seen on the surface of the $DyFeO_3$ crystal which might have been obstructed by the microdisc

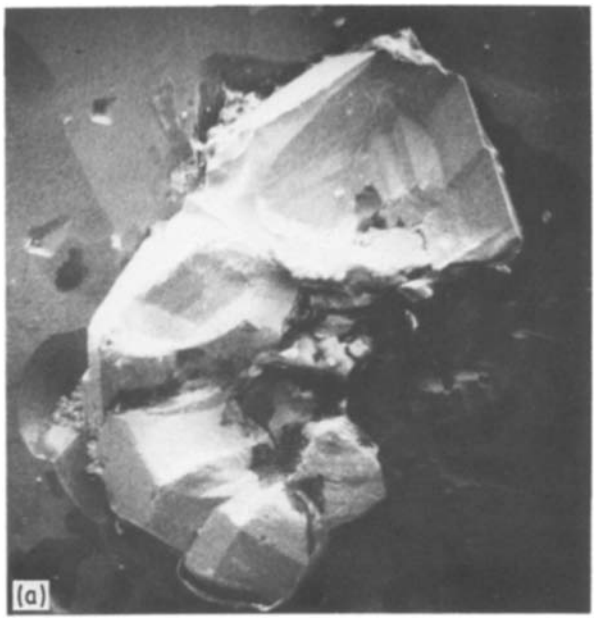

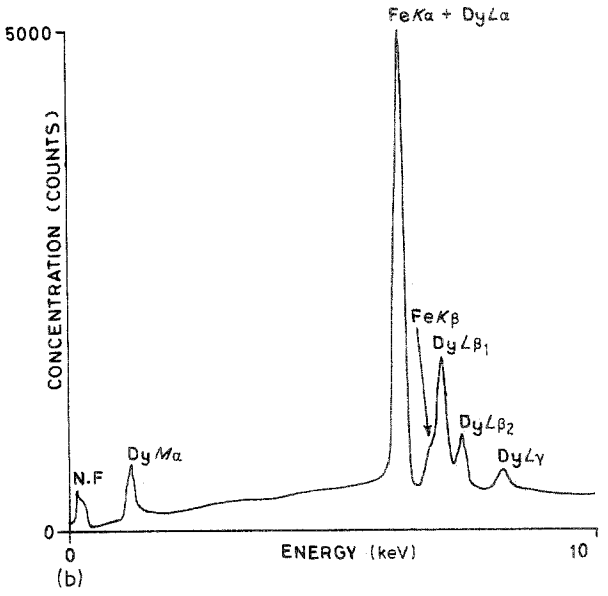

Figure 10 (a) Attached guest microcrystals on the host surface of a growing $DyFeO_3$ crystal (× 44). (b) Energy-dispersive X-ray spectrum recorded on the microcrystals of (a) revealing the composition ($DyFeO_3$).

during the process of their advancement. Formation of a microdisc rich in lead is unlike the observations reported so far for other flux-grown rare-earth orthoferrites [14, 15]. It is also very unusual in the present case because all the other microdiscs observed during the present study on $DyFeO_3$ crystals (irrespective of which batch they belong to) are circular (and not elliptical) and are made of the same material as the general surface ($DyFeO_3$). This example offers evidence of the precipitation of material containing lead during the flux growth of $DyFeO_3$, and connects the formation of microdiscs with the precipitation of secondary phases as suggested by the authors in the case of other flux-grown rare-earth orthoferrites [14, 15].

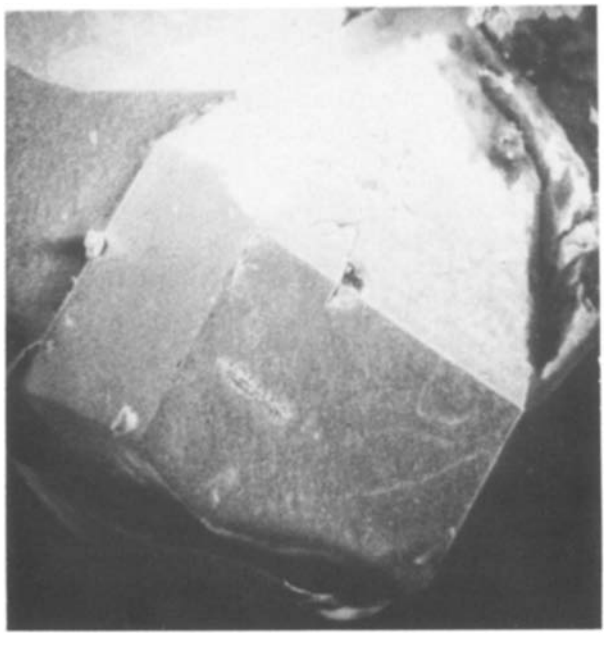

Figure 11 An electron micrograph showing one of the guest microcrystals of Fig. 10 at a higher magnification, revealing its morphology (× 180).

3.2. Results on Batch B

Fig. 16 is an optical micrograph showing irregular structures on a surface of $DyFeO_3$, which appear to be due to some impurity phases shown under the SEM in Fig. 17. The structures are highly irregular both in their contour as well as in content.

The material within the central regions seems to be different from the peripheral portions and also appears to be loosely packed inside the rest of the structure. One can also identify structures (such as that marked A in Fig. 17) with hollow central portions. It appears very logical to assume that the loosely packed material in the central region of such a feature might have fallen off from the structure. In order to understand the formation of these structures, it is necessary that the phases composing them are identified. In order to make this investigation, one of the structures of Fig. 17 was selected. Fig. 18a is an electron micrograph showing one of the irregular elevated structures of Fig. 17. A critical study reveals

Figure 12 A scanning electron micrograph showing depressions on the host surface of $DyFeO_3$ (× 50).

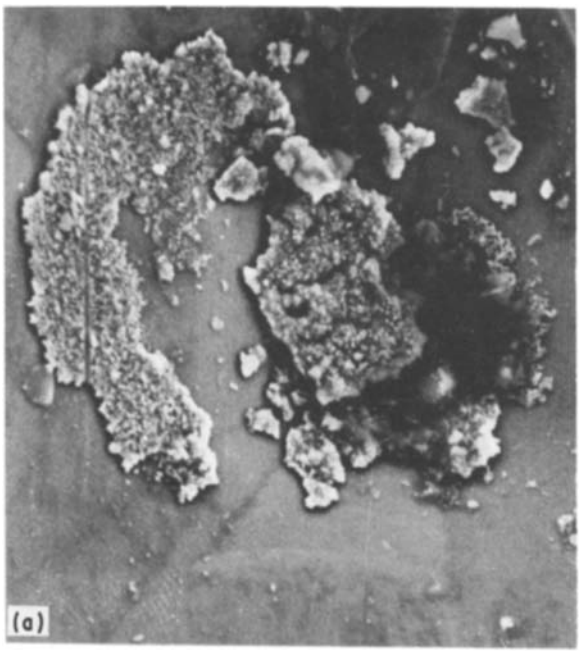

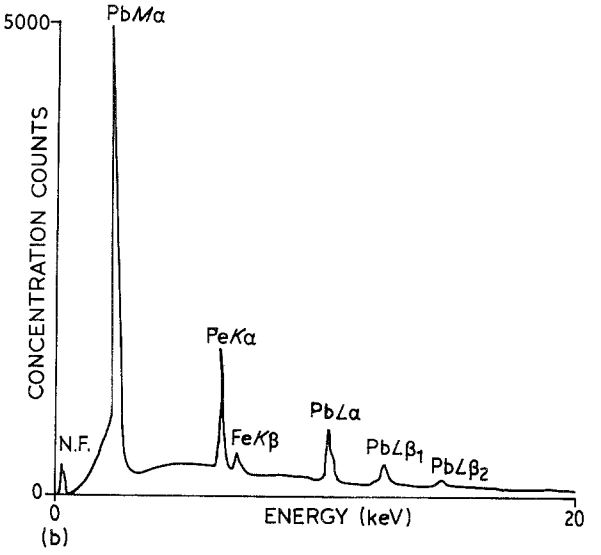

Figure 13 (a) Precipitated material in the form of cluster of small grains in the vicinity of the depressions as viewed under SEM (× 1920). (b) Energy-dispersive X-ray spectra recorded on the grains of (a) indicating the precipitation of magnetoplumbite ($PbO \cdot 6Fe_2O_3$) on $DyFeO_3$ crystal surfaces.

the structure as consisting of two parts:

(i) One is apparently a loosely-packed material in the central region of the feature as indicated by an arrow.

(ii) The other part is the peripheral one surrounding the so-called central region and is more firmly packed.

X-ray mapping of the corresponding region of Fig. 18a shown in Figs 18b and c indicates the following:

(i) There is an absence of Dy$L\alpha$ and Fe$K\alpha$ in the central region of the feature, whereas the more compact mass outside the marked region (the so-called peripheral region) illustrates the detection of Dy$L\alpha$ and Fe$K\alpha$ radiation (Fig. 18b), confirming the central region to be devoid of dysprosium and iron.

(ii) The central region of the irregular structure illustrates the detection of Pb$M\alpha$ radiation (Fig. 18c), confirming this portion of the irregular structure to be rich in lead. The peripheral part of the structure shows a near-absence of lead in much the same way as for the rest of the $DyFeO_3$ crystal surface.

From these observations, it becomes clear that the irregular structures of Fig. 17 essentially owe their origin to the precipitation of two phases, material containing lead (probably flux) and $DyFeO_3$; this particular formation takes place almost at the end of normal development of the bulk $DyFeO_3$ crystal. The loosely packed material is material containing lead whereas the more compact formation is $DyFeO_3$, probably resulting from particles of flux left after hot-pouring which deposited $DyFeO_3$ in the shape shown (for example) at A in Fig. 17.

Fig. 19a shows an irregular elevated structure consisting mainly of two parts A and B connected by a strip C. The height of the part A is greater than the heights of the strip C and the part B. X-ray mapping micrographs of the corresponding region of Fig. 19a are shown in Figs 19b and c. Fig. 19b is the corresponding region of Fig. 19a when the spectrometer was set for the detection of Dy$M\alpha$ radiation, whereas Fig. 19c is the one when the spectrometer was set for Fe$K\alpha$ radiation. The X-ray mapping (Figs 19b and c) clearly reveals the following:

(i) Dysprosium is present all over the surface including the irregular growth structures and the general background structures (Fig. 19b).

(ii) The regions A and C contain both dysprosium as well as iron, like the rest of the $DyFeO_3$ crystal surface.

(iii) The elevated region B is rich in dysprosium; iron is almost absent.

In this batch of crystals B_2O_3 is not present in the starting composition for $DyFeO_3$ growth. The precipitation of DyOF is supported by the fact that these features do not disappear on acid (HNO_3) treatment. It could not be metallic dysprosium because this metal is far too reactive.

Fig. 20a shows macro- and micro-disc patterns on a crystal surface of this batch. The discs are covered with lead impurities especially at the peripheries.

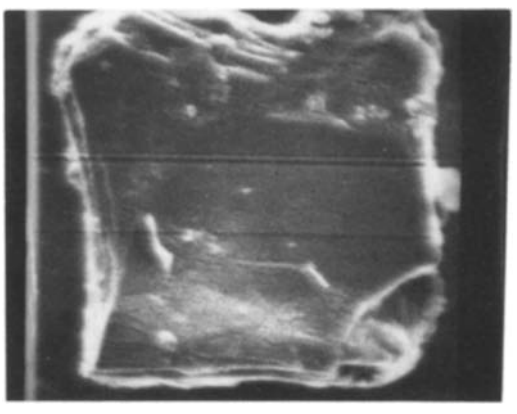

Figure 14 An electron micrograph showing large inclusions in a $DyFeO_3$ crystal (× 50).

Elliptical features are seen on the surface of a micro-disc as well as on the general surface. The elliptical features have been confirmed to be composed of $DyFeO_3$ by the EDAX technique, as shown in Fig. 20b Both macro- as well as micro-discs are composed of $DyFeO_3$. Critical examination revealed that the growth fronts of $DyFeO_3$ are modified on crossing over the disc. This observation suggests that the macro- and micro-disc formation took place before the growth of $DyFeO_3$ had ceased. Precipitation of material containing lead (which could be $PbO \cdot 6Fe_2O_3$) and its adherence at the peripheries of the discs seem to be a subsequent development. The formation of the disc is suggested to be due to droplets of fluxed melt adhering to the surface after hot pouring. $DyFeO_3$ precipitates from the adhered drop of fluxed melt and thus a layer of $DyFeO_3$ crystallizes (the bulk crystal acting as substrate) and on further cooling $PbO \cdot 6Fe_2O_3$ precipitates.

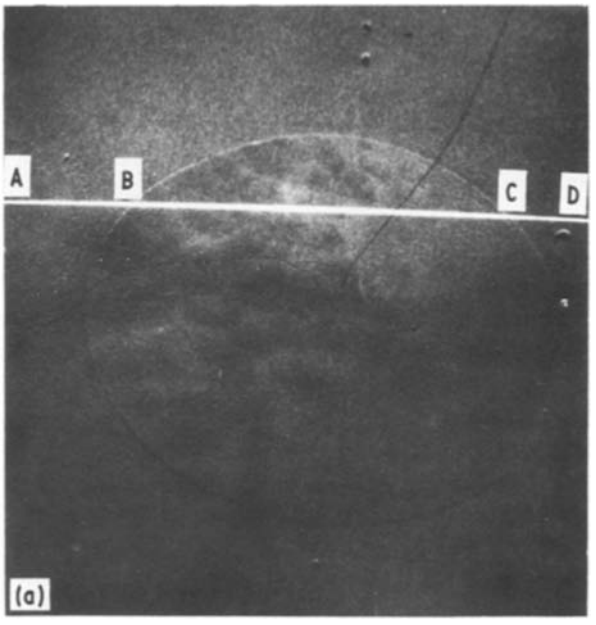

3.3. Results on Batch C

Fig. 21a shows clusters of impurity grains concentrated at some places on a $DyFeO_3$ crystal surface. Such formations result in irregular elevated regions. X-ray mapping micrographs of the corresponding region of Fig. 21a are shown in Figs 21b and c. It was verified that iron was present throughout, whether on the general surface or the precipitated impurity grains. Fig. 21b shows the corresponding region of Fig. 21a when the spectrometer was set for detecting Dy$M\alpha$ radiation, whereas Fig. 21c was recorded when the spectrometer was adjusted for recording Pb$M\alpha$ radiation. The X-ray mapping reveals the following:

(i) The clusters of grains are a secondary phase which does not contain dysprosium, Dy$M\alpha$ signals

Figure 15 (a) Scanning electron micrograph showing a typical elliptical-shaped microdisc. The white line (A–B–C–D) across it is the route along which elemental scanning was done ($\times 50$). (b) Element profile obtained on scanning of (a), showing distributions of the elements lead, iron and dysprosium as we go from left to right along the horizontal white line across (a). The traces correspond to Pb$M\alpha$, Fe$K\beta$ and Dy$L\beta$ radiations. Note the lead-rich region BC covering the elliptical microdiscs.

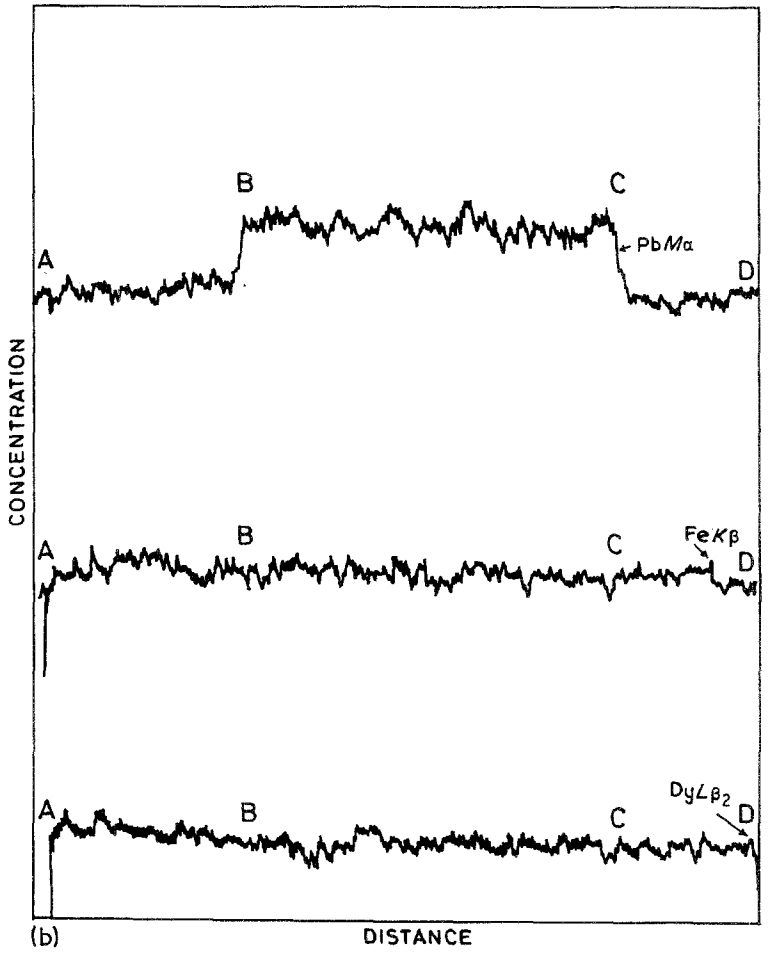

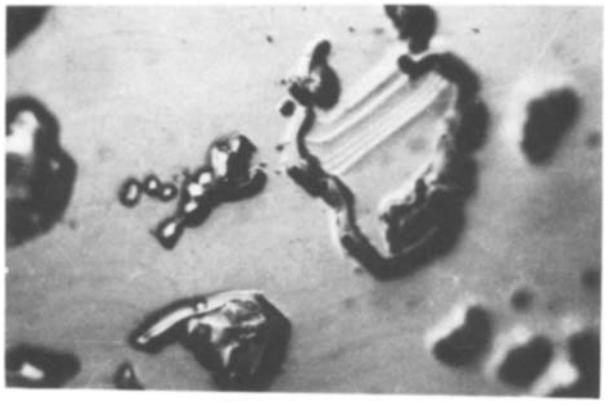

Figure 16 An optical micrograph showing irregular structures of some impurity phases on a $DyFeO_3$ crystal surface (× 48).

being completely absent for the precipitated material (Fig. 21b).

(ii) The precipitated material is rich in lead, Pb$M\alpha$ signals being predominantly present in the regions occupied by the precipitated material (Fig. 21c).

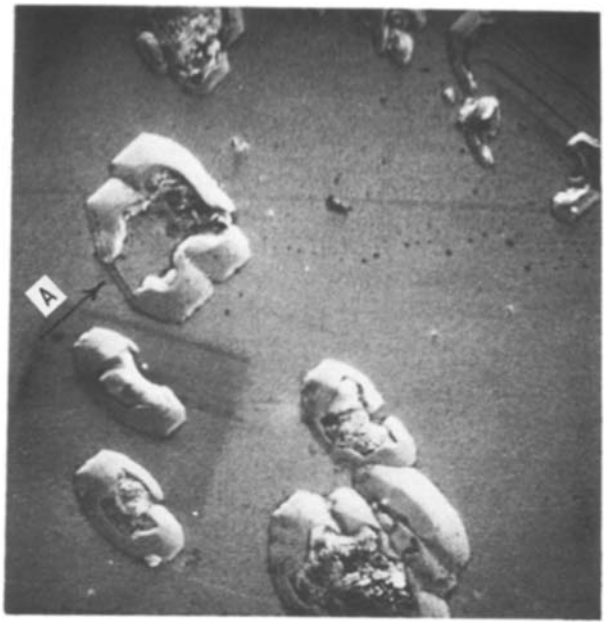

Figure 17 An electron micrograph showing some elevated structures which are highly irregular both in their contour as well as their content. The structures consist of two different phases; one type in the central region is loosely packed and the other type, lying in the peripheral portion, is more compact. Note hollow central portions (marked A) created by fallout of loosely packed phase (× 445).

(iii) Iron is present in the precipitated material, there being no distinction in Fe$K\alpha$ signals so far as the regions occupied by the clusters of grains (secondary precipitation) and the general surface are concerned.

The study confirms the precipitated material to be magnetoplumbite ($PbO \cdot 6Fe_2O_3$). Examination

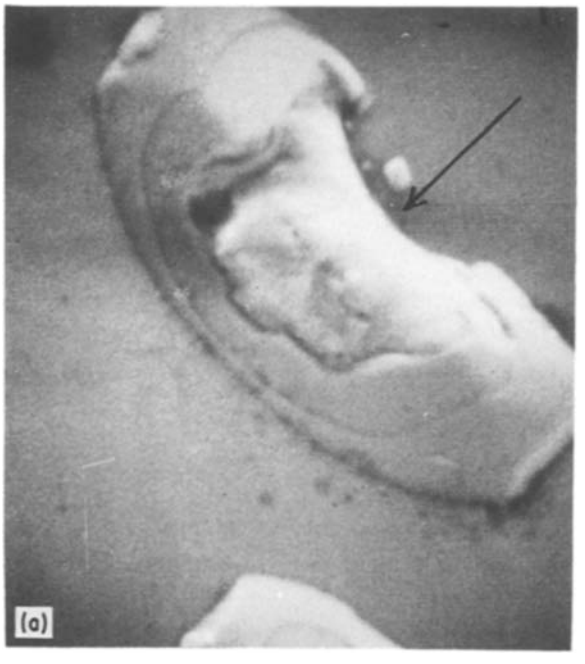

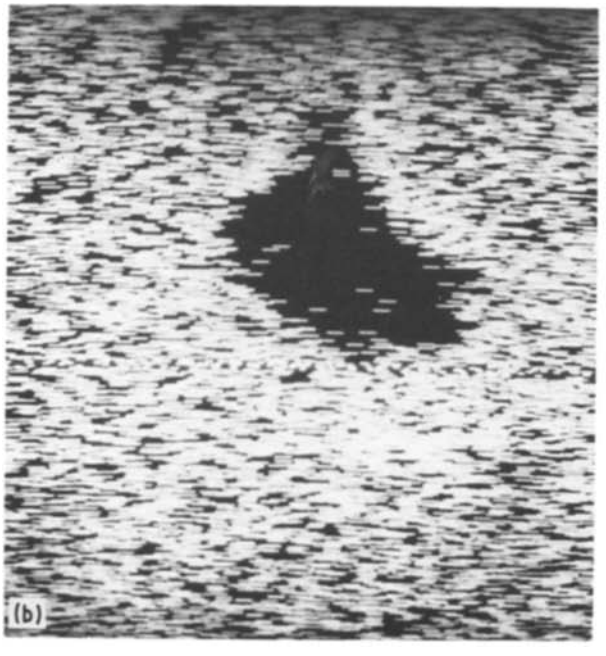

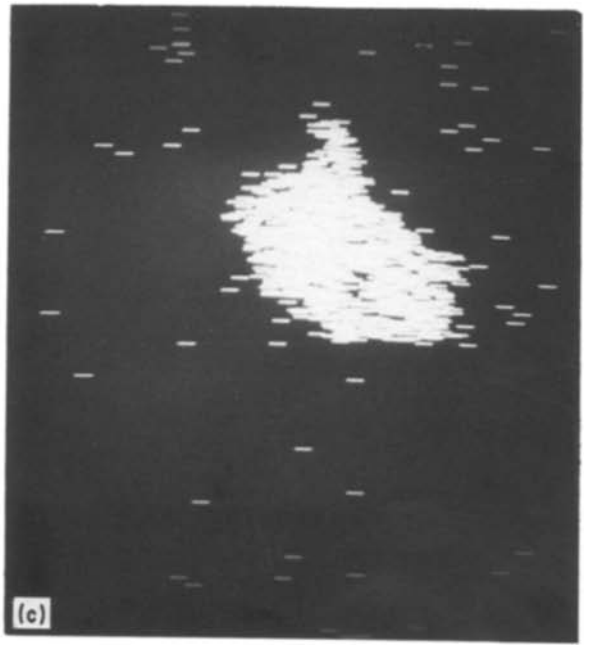

Figure 18 (a) An electron micrograph showing one of the elevated structures composed of two phases of Fig. 17, revealing its finer details. (b) Energy-dispersive X-ray micrograph of the region shown in (a) indicating absence of Dy$L\alpha$ and Fe$K\alpha$ radiation in the central region of the feature, whereas the peripheral region (surrounding the central loosely packed region) indicates the presence of both. This confirms the central region to be devoid of dysprosium and iron. (c) X-ray micrograph revealing the detection of Pb$M\alpha$ radiation, confirming this portion of the elevated structure to be rich in lead. All × 1920.

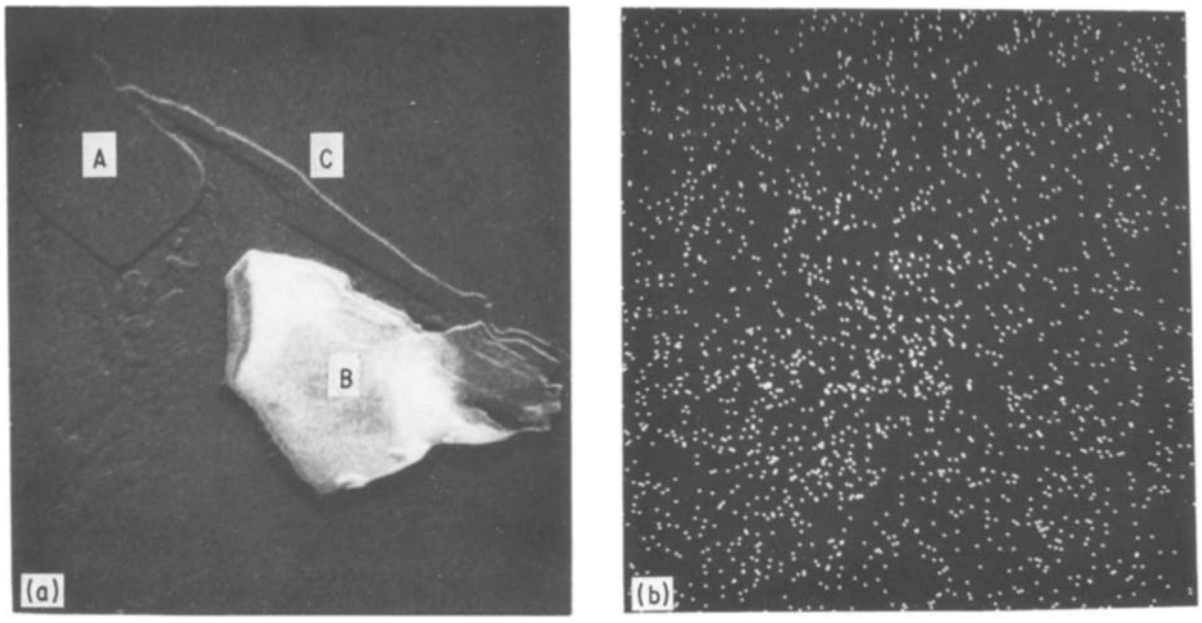

Figure 19 (a) Scanning electron micrograph showing typically elevated irregular structure consisting of two parts A and B connected by a strip C. (b) Energy-dispersive X-ray micrograph of (a) detecting Dy$M\alpha$ radiation, confirming the presence of dysprosium all over the surface including the elevated structures. (c) X-ray micrograph detecting Fe$K\alpha$ radiation, confirming the part B to be deficient in iron. All $\times 450$.

of regions surrounding the clusters indicates their formation at the end of $DyFeO_3$ growth.

3.4. Results on Batch D

Fig. 22 shows a prismatic crystal platelet (microcrystal) on a $DyFeO_3$ crystal surface. EDAX studies indicated the microcrystal to be rich in dysprosium, iron being absent. The microcrystal could be $DyBO_3$ or $DyVO_4$ (the flux composition contains both B_2O_3 as well as V_2O_5). The possibility of the microcrystal being $DyBO_3$ is ruled out because acid treatment of the crystal did not dissolve it; $DyBO_3$ will dissolve in acid whereas $DyVO_4$ will not. Also the microcrystal has the typical habit of flux-grown $DyVO_4$. It is inferred that the microcrystal is $DyVO_4$ which has nucleated and grown as a crystal platelet at the $DyFeO_3$ crystal surface.

Fig. 23 is an optical micrograph showing a macrodisc of $DyFeO_3$ but covered with an impurity composed of magnetoplumbite containing traces of vanadium, as revealed by EDAX traces. Attention may be drawn to the fact that the growth fronts of

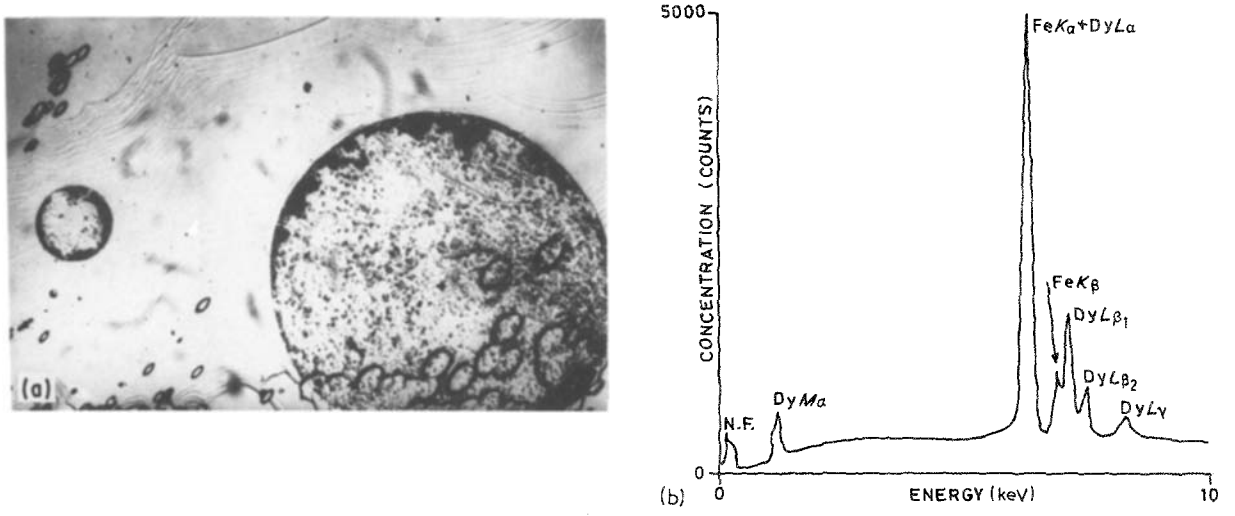

Figure 20 (a) An optical micrograph showing macro- and micro-disc patterns on a $DyFeO_3$ crystal surface. Note lead impurities and elliptical features over the surfaces of discs ($\times 48$). (b) EDAX trace recorded on the elliptical structures of (a) confirming their composition to be the same as that of general surface ($DyFeO_3$).

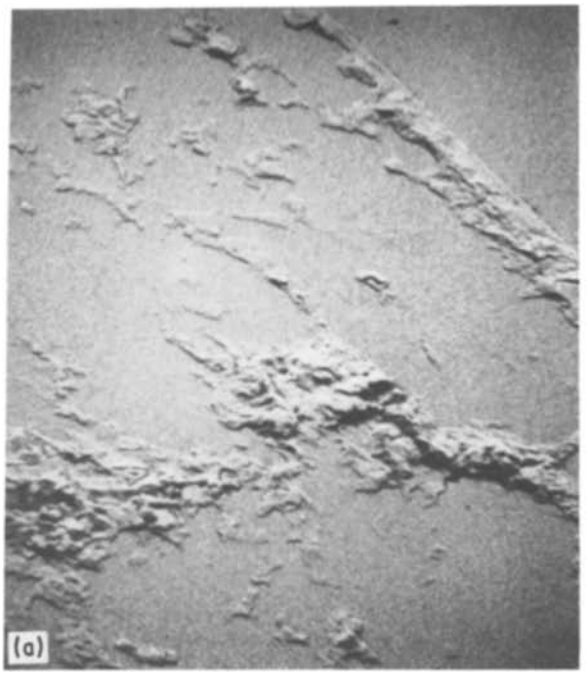

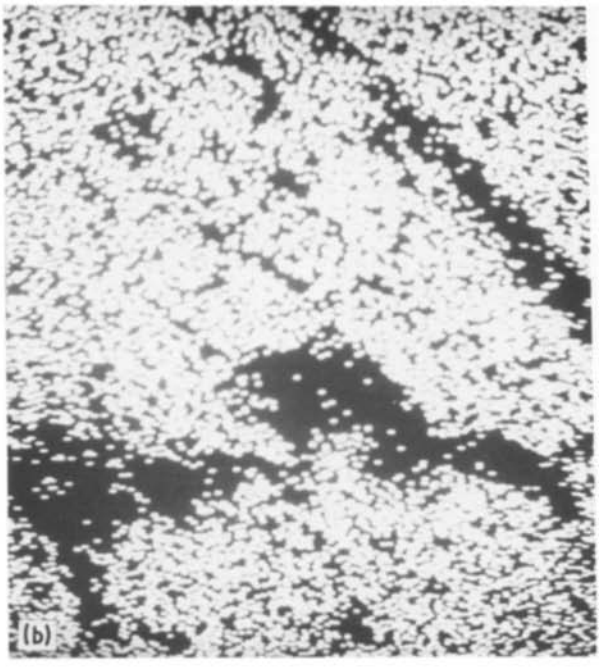

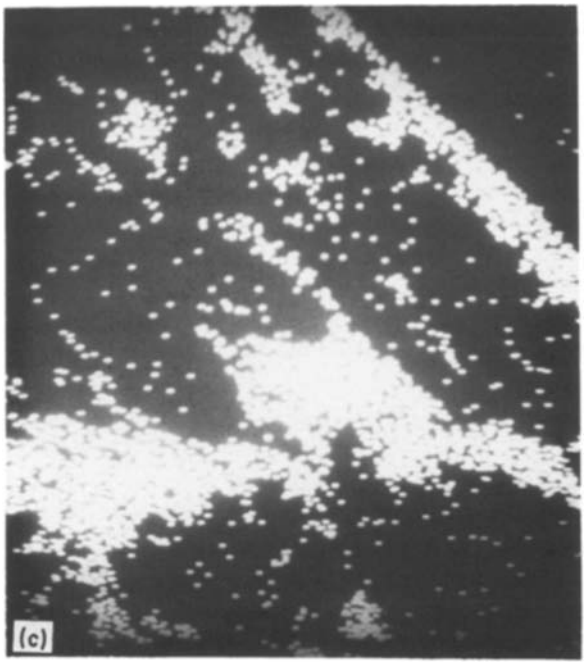

Figure 21 (a) An electron micrograph illustrating clusters of impurity grains concentrated on a $DyFeO_3$ crystal surface. (b) X-ray mapping micrograph of the corresponding region of (a) detecting Dy$M\alpha$ radiation, confirming the absence of dysprosium in the clusters. (c) X-ray mapping micrograph of the corresponding region of (a) detecting Pb$M\alpha$ signals, confirming the clusters to be rich in lead. All × 500.

$DyFeO_3$, generated by some initiating centres of growth on the general $DyFeO_3$ crystal surface, get kinked on riding over the macrodisc. This observation is indicative of macrodisc formation during the crystal growth of $DyFeO_3$. The adherence of impurities rich in lead and iron and with small traces of vanadium seems to be a subsequent development. This is supported by the fact that the growth fronts on the macrodisc are blanked out from observation in those regions which are covered by the impurities. The growth fronts on the macrodisc are clearly visible in clean regions. It seems quite logical to attribute the origin of this macrodisc to be a droplet of fluxed melt adhering to the surface on hot pouring. Here (where the separation from flux is done by the hot-pouring process) eutectic solidification did not occur in the presence of the crystals. The flux was poured off the crystals before it solidified, by inverting the crucible. There is a possibility of drops of flux sticking to the surface and depositing a macrodisc, or leaving attached flux between crystal and crucible. It is believed that $DyFeO_3$ precipitates from the adhered drop of fluxed melt, and thus a layer of $DyFeO_3$ crystallizes on the bulk crystal which acts as a substrate. Thin deposition of $DyFeO_3$ may also be taking place on the general surface. On further cooling, $PbO \cdot 6Fe_2O_3$ precipitates. This appears to be a very logical explanation for the formation of the macrodisc of Fig. 23 (see also Fig. 20). It is significant that macrodiscs are only seen on crystals where hot pouring has taken place. The interpretation given here for the formation of

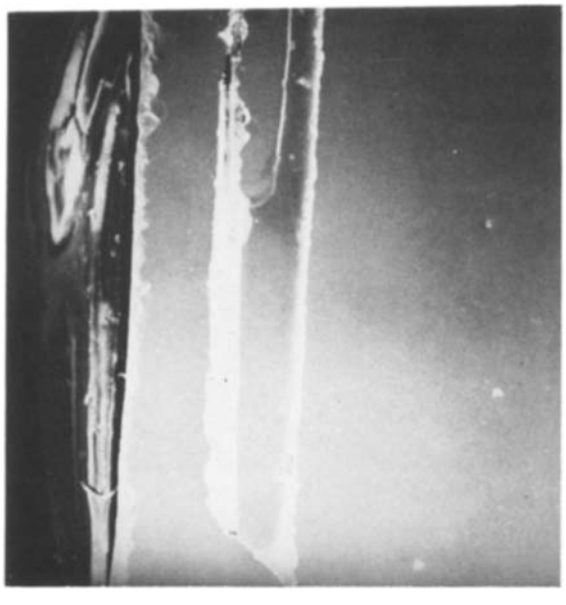

Figure 22 Prismatic crystal platelet of $DyVO_4$ attached to a $DyFeO_3$ crystal surface. (× 50).

TABLE II Summary of observations on the $DyFeO_3$ crystal surfaces

Batch	Structure	Figs	Technique*	Analysis	Conclusion	Further notes
A	Elevated structures with three straight and one curved sides. Grains at the two extreme regions or along sloping sides	1 to 9	OM/SEM/EPA	Features rich in dysprosium and deficient in iron. The grainy material is platinum. The structures dissolve in acid.	Secondary phase $DyBO_3$ likely (elevated structures). Platinum is precipitated as grainy material.	Formed after growth of $DyFeO_3$ had ceased. Attachment of platinum grains is a subsequent development found at isolated sites, in arrays and fused together. Probably platinum dissolved in the flux, precipitating at eutectic crystallization.
	Microcrystals	11	SEM/EDAX	Same peaks in EDAX as the flat surface of $DyFeO_3$.	Microcrystals of $DyFeO_3$ attached to host surface of bulk $DyFeO_3$ crystals, due to fast cooling from 850° C to eutectic.	Microcrystal morphology almost similar to the main single crystals of $DyFeO_3$.
	Cavities	12, 13	SEM/EDAX	Impurities at base of cavities show peaks of lead and iron only. Dysprosium peaks absent.	Crystallization of magnetoplumbite ($PbO \cdot 6Fe_2O_3$)	Cavities are formed by the detachment of guest microcrystals of $DyFeO_3$ from the general host surface of bulk $DyFeO_3$.
	Large inclusions	14	SEM		Secondary phase (probably $PbO \cdot 6Fe_2O_3$) having entered the crystal as a large inclusion	
	Elliptical-shaped microdiscs	15	SEM/EPA	Feature rich in lead. Dysprosium and iron also present.	Microdisc composed of impurity phase (most probably undissolved or incompletely dissolved flux)	Rare observation. Microdiscs exhibited by other rare-earth orthoferrites ($RFeO_3$ where R = Er, Ho) [14, 15] and other batches of $DyFeO_3$ reported here are composed of $RFeO_3$.
B	Irregular structures stuffed with loosely packed material in the central region	16 to 18	OM/SEM/XM	Material within the central region contains lead; dysprosium and iron are absent. Outer boundaries contain dysprosium and iron.	Structures composed of two different phases. Loosely packed central part contains lead (most likely, residues of flux) and the peripheral part is $DyFeO_3$.	Formation at the end of normal development of $DyFeO_3$ crystals.
	Irregular elevated structures in the dumbell shape	19	SEM/XM	One part exhibits presence of (Dy + Fe) whereas the other part shows only dysprosium (iron absent). The feature does not dissolve in acid.	One part due to preferential growth of $DyFeO_3$ and the other part is DyOF.	Possibility of $DyBO_3$ ruled out.
	Micro- and macro-discs	20	OM/EDAX	Discs show dysprosium and iron as main constituents. Impurities at their peripheries are rich in lead.	Discs are composed of $DyFeO_3$. $PbFe_{12}O_{19}$ impurity adheres mainly to their peripheries.	Formation of disc due to a droplet of fluxed melt adhering to the surface after hot pouring. $DyFeO_3$ precipitates from the adhered drop of fluxed melt, thus a layer of $DyFeO_3$ crystallizes (the bulk crystal acting as substrate) and on further cooling $PbO \cdot 6Fe_2O_3$ precipitates.
C	Irregular elevations (due to cluster of impurity grains)	21	SEM/XM	Secondary phase, rich in lead and iron, dysprosium absent.	Crystallization of $PbO \cdot 6Fe_2O_3$	Formation (at the end of $DyFeO_3$ crystal growth) after hot pouring.

TABLE II *Continued*

Batch	Structure	Figs	Technique*	Analysis	Conclusion	Further notes
D	Attached guest prismatic crystal platelet (microcrystals)	22	SEM/EDAX	Rich in dysprosium; iron absent.	Crystallization of single crystal $DyVO_4$ likely. $DyBO_3$ dissolves in acid, whereas $DyVO_4$ does not.	The shape of the microcrystal corresponds to the typical flux-grown habit of $DyVO_4$. The guest microcrystal nucleates at the host surface of the $DyFeO_3$ crystal.
	Microdisc	23	OM/EDAX	Macrodisc contains dysprosium and iron (same as on $DyFeO_3$ general surface); impurities covering it composed of lead, iron and traces of vanadium.	Macrodisc of $DyFeO_3$. Precipitation of $PbO \cdot 6Fe_2O_3$ likely. Impurity phase adhering to the macrodisc develops after growth of a layer of $DyFeO_3$.	Formation due to droplet of fluxed melt adhering to the surface after hot pouring. $DyFeO_3$ precipitates from the adherent drop of flux and thus a layer of $DyFeO_3$ crystallizes on the bulk crystal which acts as a substrate. On further cooling, $PbO \cdot 6Fe_2O_3$ precipitates.

*OM: optical microscopy, EPA: elemental profile analysis, XM: X-ray mapping, SEM: scanning electron microscopy, EDAX: energy dispersive analysis of X-rays.

Figure 23 An optical micrograph showing a macrodisc of $DyFeO_3$ (on a $DyFeO_3$ crystal surface) covered with the impurities composed of lead, iron and small traces of vanadium ($\times$ 50).

macrodiscs is further supported by the observation that before cleaning in acid, the round lump of flux is easily seen.

The results obtained on crystals of $DyFeO_3$ grown under various growth conditions (starting composition, cooling rate, soaking period, maximum temperature etc.) are summarized in Table II.

Irrespective of what the growth conditions are, precipitation of secondary phases occurs during the flux growth of $DyFeO_3$. Crystallization of magnetoplumbite ($PbO \cdot 6Fe_2O_3$) is very common; it is detected in three batches (A, C and D) though they are grown under varied conditions. Precipitation of an impurity containing lead (most probably $PbFe_{12}O_{19}$ and/or Pb_2OF_2) is indicated in two batches (A and B). Formation of DyOF is observed only on the crystals of Batch B. Crystallization of a secondary phase of composition $DyBO_3$ is indicated in Batch A and of $DyVO_4$ in Batch D. The presence of B_2O_3 for Batch A results in the formation of $DyBO_3$ during $DyFeO_3$ crystal growth. Addition of V_2O_5 in the flux system for Batch D results in the crystallization of $DyVO_4$. Microcrystals of $DyFeO_3$ attached to the host crystal are observed for Batch A, no doubt precipitated during rapid cooling below 850° C. Batch A also offers the rare observation of a microdisc containing lead (probably undissolved or incompletely dissolved flux), whereas the other batches (B and D) show discs made of $DyFeO_3$ (i.e. of the same composition as the bulk crystal).

Significantly, it is only Batch A which revealed the presence of platinum. It is well known that PbO attacks platinum severely, while PbF_2, alone or with PbO, is much less corrosive. High temperatures (above 1200° C) may lead to solution of platinum, followed by its deposition in or on a growing crystal. In an experiment performed at 1330° C, Wanklyn [16] has reported solution and transport of platinum leading to deposition of a thick layer of platinum on the upper wall of the crucible. Deposition of platinum as fine grains on the $DyFeO_3$ crystals is attributed to the crystals being cooled through the eutectic in contact with the flux, whereas the other batches were separated from the molten flux. This inference is drawn from the fact that the presence of platinum occurs on the $DyFeO_3$ crystals of Batch A only. This deposition of platinum is especially interesting because induction times in differential thermal analysis experiments have been explained in terms of platinum being dissolved at higher temperatures and being precipitated at eutectic crystallization, thus replacing nucleation sites [17]. The present study thus confirms that hypothesis. The crystals of Batch A also show the precipitation of more types of secondary phase and more imperfections in crystals. The separation of flux in this batch was done by tapping with a hammer, which might have forced some of the attached microcrystals to become detached from the host $DyFeO_3$ crystal surface, thus resulting in cavities. In this respect, the hot-pouring technique for separation of flux is preferable.

4. Conclusions

1. Using the PbO–PbF_2–B_2O_3 flux system for the growth of $DyFeO_3$ results in the precipitation of magnetoplumbite ($PbO \cdot 6Fe_2O_3$) as a secondary phase even under varied starting composition and thermal conditions.

2. Deposition of platinum as fine grains on the $DyFeO_3$ crystal results when the crystal is cooled through the eutectic in contact with the flux. This deposition does not occur if the crystals are separated from the molten flux.

3. Other secondary phases, DyOF and $DyBO_3$, are also precipitated; more DyOF is produced when B_2O_3 is not included in the flux system. $DyVO_4$ occurs as single crystals on the $DyFeO_3$ crystal surfaces when V_2O_5 is present.

4. Addition of V_2O_5 to the PbO–PbF_2–B_2O_3 flux system leads to the incorporation of small traces of vanadium in the $DyFeO_3$ crystal.

5. Besides the precipitation of secondary phases as inclusions, discs, irregular and regularly shaped elevated structures, microcrystals and grains, there are extraordinary regions where the growth of $DyFeO_3$ itself occurs in the form of macrodiscs. These are due to a droplet of fluxed melt adhering to the surface after hot pouring. $DyFeO_3$ then precipitates from the adherent droplet of fluxed melt and thus a layer of $DyFeO_3$ crystallizes, with the bulk crystal acting as substrate. On further cooling, $PbO \cdot 6Fe_2O_3$ also precipitates.

Acknowledgements

One of us (S.K.K.) is grateful to UGC (India) for the award of a Research Fellowship. The research work is supported by the UGC (India). We wish to express our thanks to Dr G. Garton, Head of the Crystal Growth Group, Clarendon Laboratory, University of Oxford, for his encouragement in the collaborative research programme between the Physics Department, University of Jammu and his Laboratory. Our thanks are also due to Mr V. G. Shah of PRL, Ahmedabad, for his help in the electron microscope work.

References

1. M. S. JOSHI and A. S. VAGH, *Indian J. Pure Appl.*

Phys. **5** (1967) 318.
2. M. S. JOSHI and P. N. KOTRU, *Jpn J. Appl. Phys.* **7** (1968) 700.
3. *Idem, Amer. Mineral.* **53** (1968) 825.
4. *Idem, Krist. Techn.* **11** (1976) 913.
5. *Idem, ibid.* **12** (1977) 13.
6. M. S. JOSHI, P. N. KOTRU and A. S. VAGH, *J. Cryst. Growth* **2** (1968) 329.
7. *Idem, Krist. Techn.* **15** (1980) 1003.
8. M. S. JOSHI and R. K. TAKU, *Indian J. Pure Appl. Phys.* **10** (1962) 34.
9. K. SANGWAL and A. R. PATEL, *J. Cryst. Growth* **23** (1974) 282.
10. P. N. KOTRU, *Jpn J. Appl. Phys.* **12** (1973) 790.
11. *Idem, Krist. Techn.* **13** (1978) 35.
12. P. N. KOTRU and K. K. RAINA, *ibid.* **17** (1982) 1077.
13. K. KIJIMA, N. MIYAMATO and J. NISHIZAWA, *J. Appl. Phys.* **42** (1971) 486.
14. P. N. KOTRU, S. K. KACHROO and B. M. WANKLYN, *J. Mater. Sci.* **21** (1986) 1609.
15. *Idem, ibid.* **21** (1986) 3625.
16. B. M. WANKLYN, in "Crystal Growth", Vol. 1, edited by B. R. Ramplin (Pergamon, Oxford, 1974) p. 217.
17. B. M. WANKLYN, B. E. WATTS and V. V. FENIN, *J. Cryst. Growth* **70** (1984) 459.

Received 2 March
and accepted 29 April 1987